CONFERENCE PRE-PRINT

CONFINEMENT MODELLING OF ENHANCED PLASMA PERFORMANCE AFTER MULTIPLE PELLET INJECTIONS IN THE T.J-II STELLARATOR

V. TRIBALDOS Universidad Carlos III de Madrid Leganés, Spain Email: Victor.Tribaldos@uc3m.es

I. GARCÍA-CORTÉS, K.J. McCARTHY, B. van MILLIGEN, A. BACIERO, R. CARRASCO, T. ESTRADA, J.M. FONTDECABA, D. LÓPEZ-BRUNA, F. MEDINA, D. MEDINA-ROQUE, J.L. de PABLOS, N. PANADERO, I. PASTOR, J. DE LA RIVA, M.C. RODRIGUEZ, and TJ-II TEAM Laboratorio Nacional de Fusión, CIEMAT Madrid, Spain

J.M. REYNOLDS-BARREDO Universidad Carlos III de Madrid Leganés, Spain

O.O. CHMYGA, O.S. KOZACHEK, Institute of Plasma Physics, NSC KIPT Kharkiv, Ukraine

Abstract

Recent experiments using multi-pellet injection in NBI-heated plasmas in the TJ-II stellarator have achieved record energy confinement times that surpass predictions derived from the International Scaling law ISS04. The deep plasma fueling of pellet injection is instrumental in establishing this enhanced confinement regime, simultaneously achieving both record densities and the highest ion temperatures measured to date in TJ-II. While these observed profile modifications suggests a potential neoclassical transport mechanism, owing to its strong collisionality dependence, simultaneous measurements of reduced density and electrostatic potential fluctuations in the density gradient region indicate a turbulent transport contribution to the overall enhanced confinement. It is shown that the increased ion temperature resulting from multi-pellet injection mitigates neoclassical diffusion by transitioning the collisionality from the Pfirsch-Schlüter regime to the plateau regime and partially explains the enhanced plasma performance observed under NBI heating in the TJ-II stellarator.

1. INTRODUCTION

Recent experimental campaigns on the TJ-II stellarator have investigated the effects of multiple cryogenic hydrogen pellet injections into neutral beam injection (NBI)-heated plasmas [1,2], expanding on earlier studies focused on ablation, deposition, and fueling efficiency [3-5]. The plasmas generated through multiple pellet injections exhibit sustained record central densities, ion temperatures, and normalized β . An extensive comparison reveals a significant improvement in the plasma triple product compared to other plasma fueling methods. Notably, the plasmas show record ion temperatures and diamagnetic energy confinement times exceeding ISS04 [6] predictions.

A comparison between discharges with and without pellets reveals that deep plasma fueling results, as expected, in an increase in the line-averaged density, Fig. 1, top, and an unexpected, substantial increase in diamagnetic energy, Fig. 1, bottom. Thomson scattering data shows broader density profiles with higher central values, Fig. 2, left, and a slight change in electron temperature profiles, Fig. 2, center. Furthermore, charge-exchange recombination spectroscopy (CXRS) measurements indicate broader ion temperature profiles with notably higher central values, see Fig. 2, right. These findings suggest that the increase in diamagnetic energy is primarily attributable to the enhanced ion kinetic energy.

At the NBI beam energy of TJ-II, approximately 75% of the beam power is transferred to the electrons [2]. Hydrogen fueling due to pellet injection directly increases the density and, through collisional coupling, the electron-to-ion energy transfer $Q_{ei} \propto n_e^2 (T_e - T_i)/T_e^{3/2}$. This, as observed in the experiment, produces a slight reduction of the electron temperature. Thus, the ion temperature is determined by the balance between the higher electron-ion energy transfer and the dependence of ion confinement on the ion temperature $\tau_i(T_i)$. The measured high ion temperature indicates a weak dependence of ion confinement on T_i , which runs counter to the typical unfavorable temperature dependence of stellarator ion transport.

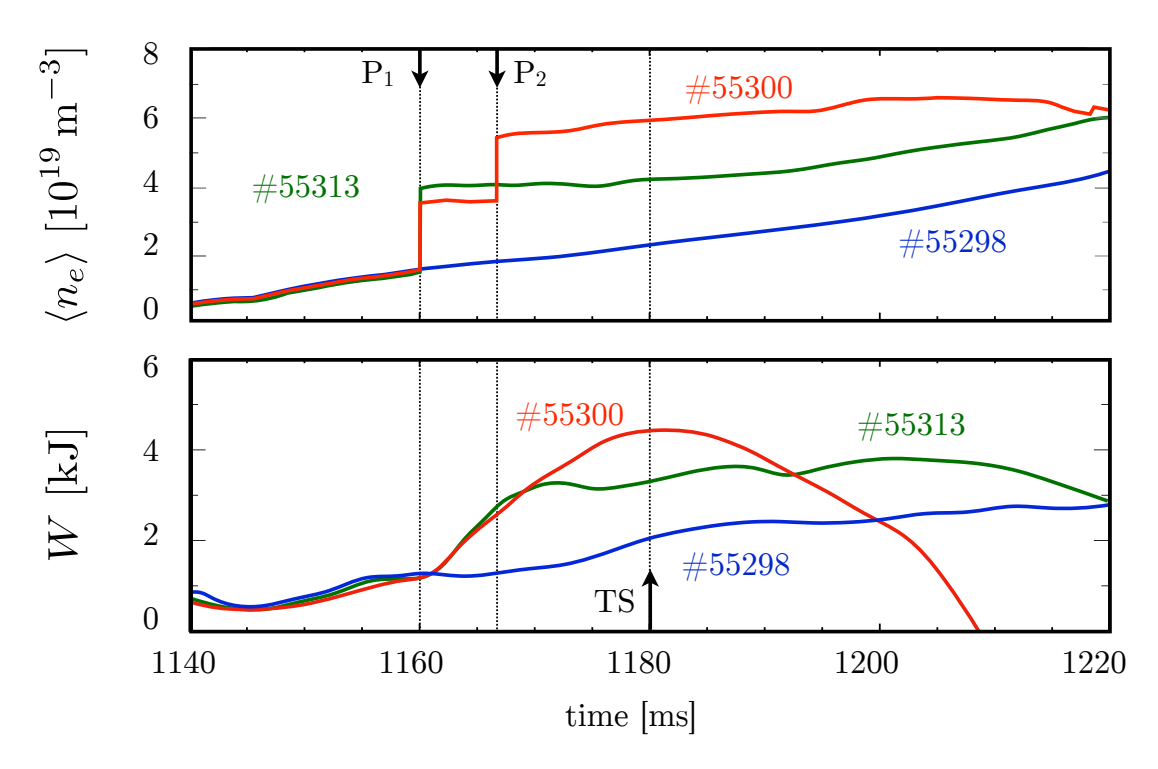


FIG. 1. Time traces of line-averaged density $\langle n_e \rangle$ and stored diamagnetic energy W for the reference discharge without pellets, #55298 (blue) and with one #55313 (green) and two #55300 (red) pellets. Pellet injection (P_1 and P_2) and Thomson scattering (TS) times are indicated with dotted lines and arrows.

The experimental findings suggest a modification in plasma transport, predominantly affecting ions. While a significant decrease in density and electrostatic potential fluctuations in the outer plasma region indicates a turbulent transport contribution [7], the more negative values of the radial electric field, measured with a Heavy Ion Beam Probe (HIBP) and CXRS, also point toward a neoclassical transport mechanism induced by pellet injection, which will be further explored in the following section.

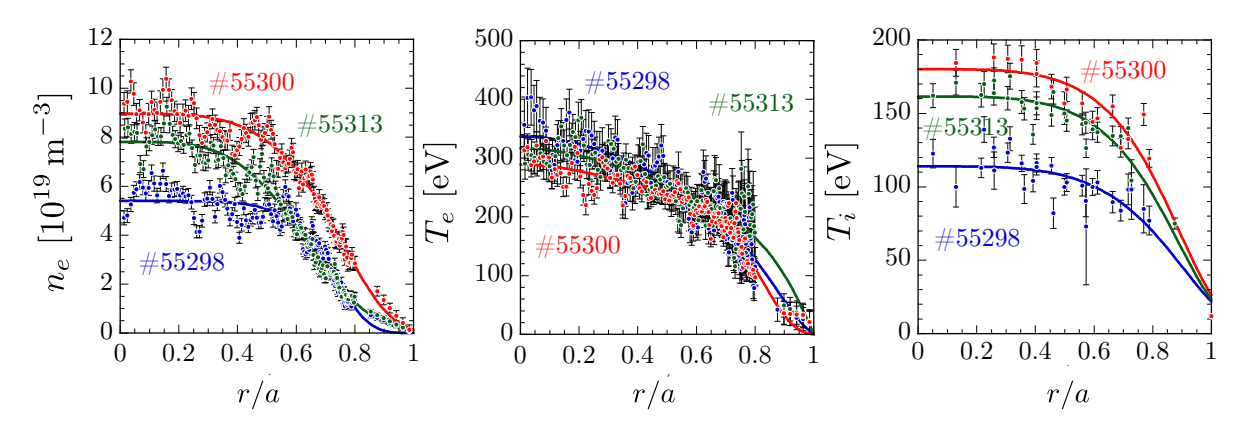


FIG. 2. Density (left), electron (middle) and ion (right) temperature profiles for the reference discharge without pellets, #55298 (blue) and with one #55313 (green) and two #55300 (red) pellets.

2. NEOCLASSICAL SIMULATIONS

To clarify the impact of neoclassical transport in this new confinement regime, simulations were performed for a series of NBI heated discharges with an absorbed $P_{\rm NBI}=320$ kW, and where the diamagnetic energy content increases from 2.4 kJ in gas-puffing-only operation, #55298, to 3.6 kJ with one pellet, #55313, and 4.4 kJ with two pellets, #55300, see Figs. 1 and 2. The neoclassical local particle Γ_{α} and energy Q_{α} fluxes and the bootstrap current densities J_{α}^{b} are calculated using the monoenergetic approach [8,9] through the three monoenergetic particle D_{11} , bootstrap D_{31} and electric conductivity D_{33} diffusion coefficients. These coefficients are computed with a combination of the codes MOCA [10] and DKES [11] for the experimental configuration $100_{-}44_{-}64$, see Fig. 3. The momentum correction technique of [12] is used to address the lack of parallel momentum conservation of the collision operator used in the monoenergetic approach. While this effect has only minor significance for radial neoclassical transport in stellarators, except at extremely high collisionalities where parallel viscous damping is minimal, it is essential for the accurate estimation of the bootstrap current. The simulation results of the radial electric field, the bootstrap current and the energy confinement time are then compared with the experimental radial electric field obtained by CXRS, the plasma current and the ISS04 and experimental power balance analysis.

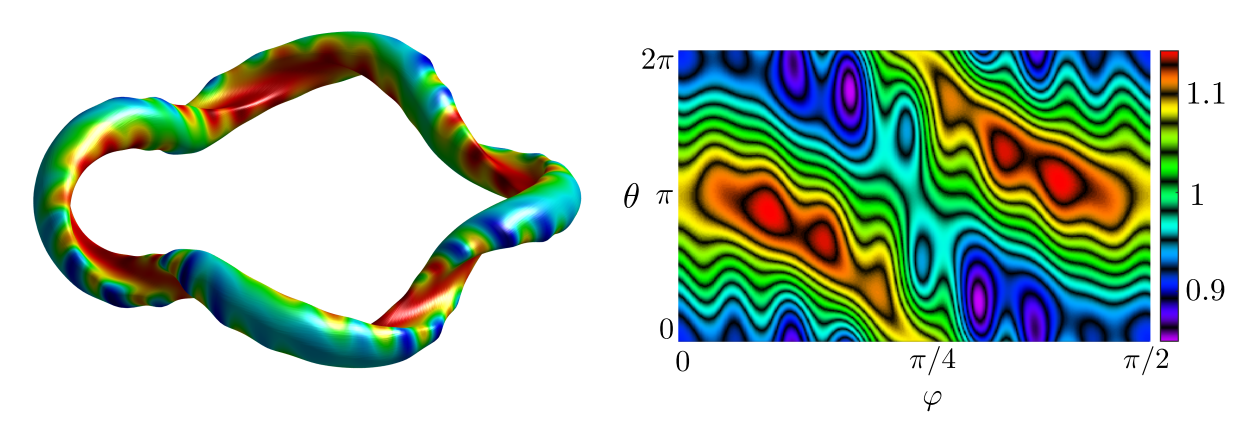


FIG. 3. Left: Magnitude of the magnetic field on the last closed flux surface for the TJ-II stellarator 100_44_64 magnetic configuration. Right: Level contours of the magnetic field magnitude at half radius, r/a = 0.5 for the same configuration, shown in Boozer coordinates (φ, θ) .

The calculation starts by precomputing, for the magnetic configuration used in the experiments, the three monoenergetic coefficient $D_{ij} = D_{ij}(r/a, \nu/v_{\alpha}, Er/v_{\alpha}B)$ for a set of plasma radial positions r/a, inverse mean free paths ν/v_{α} and normalized radial electric fields, $E_r/v_{\alpha}B$, ensuring that the radial electric field grid is made sufficiently fine to resolve, at least, the first radial electric field resonance. Second, the values of the radial electric field E_r^* , solutions of the ambipolar equation $\sum_{\alpha} Z_{\alpha} \Gamma_{\alpha}(E_r^*) = 0$, are computed at every radial position, where Z_{α} and Γ_{α} are the charge and particle flux of species α which, just keeping with the radial electric field dependence for clarity, is given by

$$\Gamma_{\alpha}(E_r) = -n_{\alpha}D_1^{\alpha}(E_r) \left[\frac{n_{\alpha}'}{n_{\alpha}} - \frac{Z_{\alpha}E_r}{T_{\alpha}} + \left(\frac{D_2^{\alpha}(E_r)}{D_1^{\alpha}(E_r)} - \frac{3}{2} \right) \frac{T_{\alpha}'}{T_{\alpha}} \right]$$

where n_{α} , T_{α} , n'_{α}/n_{α} and T'_{α}/T_{α} are the density, temperature and their logarithmic radial gradients and the D^{α}_n are the thermal particle diffusion coefficients. The *Ware* pinch term, proportional to the parallel electric field (loop voltage), is omitted because of the current-free stellarator operation. The D^{α}_n are obtained through energy convolutions of the *mononergetic* coefficients D_{11} for n=1,2,3 and D_{31} for n=4 and 5

convolutions of the *mononergetic* coefficients
$$D_{11}$$
 for $n=1,2,3$ and D_{31} for $n=4$ and 5
$$D_n^{\alpha} = \frac{2}{\pi} \int_0^{\infty} e^{-K_{\alpha}} K_{\alpha}^{n-1/2} D_{11} \, dK_{\alpha} \quad \text{and} \quad D_n^{\alpha} = \frac{2}{\pi} \int_0^{\infty} e^{-K_{\alpha}} K_{\alpha}^{n-7/2} D_{31} \, dK_{\alpha}$$

with $K_{\alpha}=m_{\alpha}v_{\alpha}^2/2T_{\alpha}$ being the normalized thermal kinetic energy. The third step consists in computing the energy fluxes $Q_{\alpha}(E_r^*)$ and the bootstrap current density $J_{\alpha}^b(E_r^*)$

$$Q_{\alpha}(E_r^*) = -n_{\alpha}T_{\alpha}D_2^{\alpha}(E_r^*) \left[\frac{n_{\alpha}'}{n_{\alpha}} - \frac{Z_{\alpha}E_r^*}{T_{\alpha}} + \left(\frac{D_3^{\alpha}(E_r^*)}{D_2^{\alpha}(E_r^*)} - \frac{3}{2} \right) \frac{T_{\alpha}'}{T_{\alpha}} \right]$$

$$J_{\alpha}^{b}(E_{r}^{*}) = -q_{\alpha}n_{\alpha}D_{4}^{\alpha}(E_{r}^{*}) \left[\frac{n_{\alpha}'}{n_{\alpha}} - \frac{Z_{\alpha}E_{r}^{*}}{T_{\alpha}} + \left(\frac{D_{5}^{\alpha}(E_{r}^{*})}{D_{4}^{\alpha}(E_{r}^{*})} - \frac{3}{2} \right) \frac{T_{\alpha}'}{T_{\alpha}} \right]$$

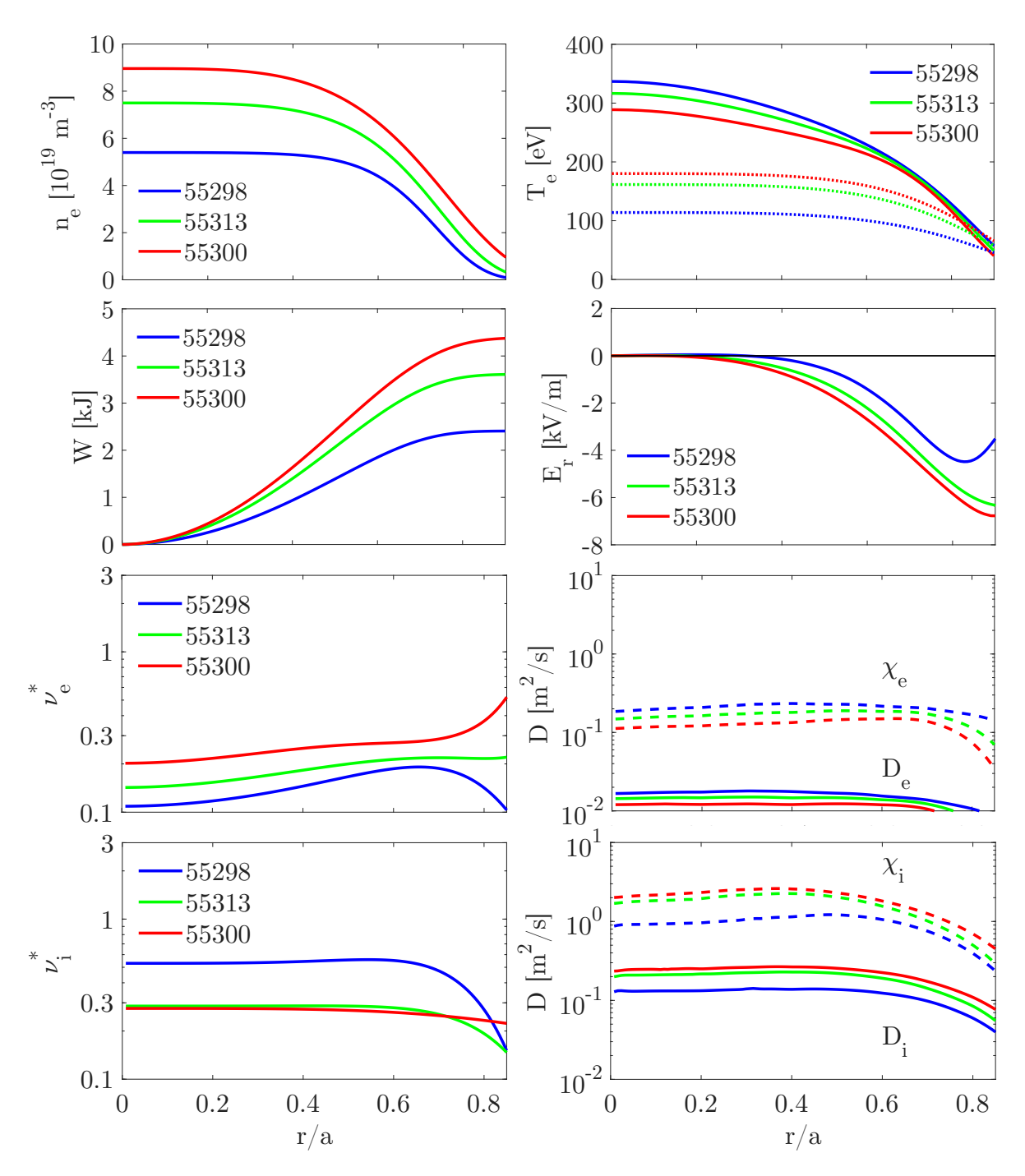


FIG. 4. From top to bottom and left to right, profiles of: electron density n_e , electron T_e (solid) and ion T_i (dotted) temperatures, integrated energy from the profiles W, ambipolar radial electric field E_r , thermal electron collisionality $\nu_e^* = \nu_e R/\nu v_{th}^e$, thermal electron diffusion D_e (solid) and heat χ_e (dotted) coefficients, ion thermal collisionality $\nu_i^* = \nu_i R/\nu v_{th}^i$ and thermal ion diffusion D_i (solid) and heat χ_i (dotted) coefficients for the reference discharge without pellets, #55298 (blue) and with one #55313 (green) and two #55300 (red) pellets.

The top four plots of Fig. 4 presents the density n_e , electron T_e , and ion T_i temperature profiles used for the three analyzed discharges, see Fig. 1. Additionally, the integrated kinetic energy $W(r) = 4\pi^2 R \sum_{\alpha} \int_0^r n_{\alpha}(r')r'dr'$ and the ambipolar radial electric field E_r^* is depicted. Notably, the radial electric field exhibits an increase to more negative values for the higher ion temperatures observed in the two pellets case, in agreement with the anticipated increased ion particle fluxes in the gradient region. Unfortunately, radial electric field measurements employing CXRS are not available for these discharges. However, measurements conducted for similar discharges reveal profiles characterized by a minimum in the same region, approximately $r/a \sim 0.8$, with values ranging from -5 to -10 kV/m. These profiles exhibit a consistent dependence on pellet injection, with more negative values observed for higher densities and ion temperatures.

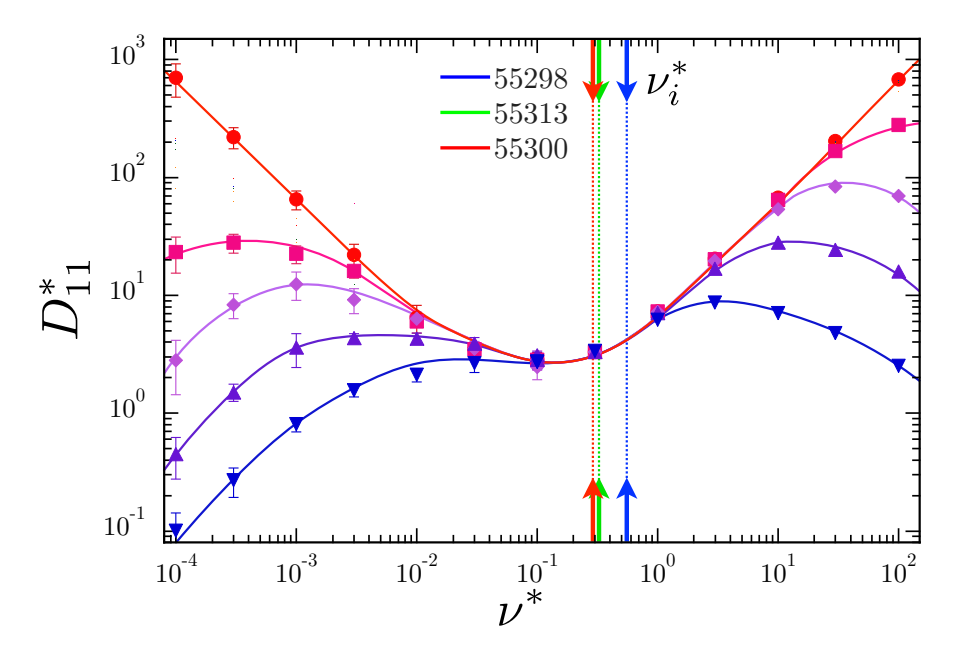


FIG. 5. Normalized monoenergetic diffusion coefficient D_{11}^* for r/a=0.5 as a function of the collisionality $\nu^*=\nu R/\iota v$, the values of ν_i^* of Fig. 5, bottom left, are shown for the three discharges analyzed.

In Fig. 4 bottom plots, the normalized collisionalities $\nu_{\alpha}^* = \nu_{\alpha} R/\nu v_{th}^{\alpha}$ and the thermal particle D_{α} and heat χ_{α} diffusivities are presented. The first finding is that, despite the electron temperature being approximately twice that of the ions in the plasma core, particle and energy ion diffusion coefficients are approximately an order of magnitude higher than their electron counterparts, exhibiting a relatively flat profile. The precision of the edge results is limited by the uncertainties in the measured plasma profiles. Comparing these values with the collisional regime of the normalized monoenergetic coefficient D_{11}^* , see Fig. 5, reveals that the ion thermal collisionality varies from the onset of the Pfirsch-Schlüter regime for the reference discharge #55298 to the plateau regime in the one- and two-pellet discharges #55313 and #55300. The first monoenergetic coefficient necessary for the convolutions $D_{11} = D_{11}^* D_{11}^p$ where $D_{11}^p = \pi v_d^2 R_0/4vi$ is the axisymmetric tokamak plateau diffusion coefficient [8].

In contrast to the behavior observed in the long mean free path (lmfp) neoclassical transport regime in stellarators, where the $D_{11}^* \propto 1/\nu^*$ and $D_n^\alpha \propto T_\alpha^{7/2}$ for n=1,2 and 3, in the Pfirsch-Schlüter regime, $D_{11}^* \propto \nu^*$ and $D_n^\alpha \propto T_\alpha^{-1/2}$. Furthermore, in the plateau regime, D_{11}^* remains independent of temperature, while $D_n^\alpha \propto T_\alpha^{3/2}$. Consequently, the relatively small reduction in collisionality in the plateau regime partially compensates for the higher ion temperature in the energy convolution of D_n^α . This explains why the thermal particle and energy diffusion coefficients, see Fig. 4, bottom right, only double for the two pellet case. Electrons lie in the plateau regime because of their slightly smaller collisionality and both the thermal electron particle and heat diffusion coefficients are remarkably similar for all discharges. Notably, in this collisionality regime the diffusion coefficients are largely independent of the radial electric field for both species, and is established by the linear $Z_\alpha E_r/T_\alpha$ term in Γ_α .

The neoclassical particle flux $\sum_{\alpha} \Gamma_{\alpha}(r/a)$ exhibit only moderate variations across the analyzed discharges, despite the significant differences in plasma density. By contrast, the surface-integrated neoclassical power $P_{NC}(r/a) \approx 4\pi^2 Ra \sum_{\alpha} Q_{\alpha}(r/a)$ increases by approximately a factor of two, driven by the enhanced energy diffusion coefficient χ_i and the higher temperature gradients. This twofold increase, however, remains consider-

ably less than might be expected given the 50% rise in ion temperature, as noted previously. Derived quantities such as the local particle and energy confinement times or the bootstrap current can be obtained through radial integration of these profiles. Using a cylindrical approximation the following expressions are obtained

$$\tau_p(r) = \frac{4\pi^2 R \sum_{\alpha} \int_0^r n_{\alpha}(r') r' dr'}{4\pi^2 R r \sum_{\alpha} \Gamma_{\alpha}(r)}, \quad \tau_E(r) = \frac{4\pi^2 R \sum_{\alpha} \int_0^r \frac{3}{2} n_{\alpha}(r') T_{\alpha}(r') r' dr'}{4\pi^2 R r \sum_{\alpha} Q_{\alpha}(r)}$$

A comparison of these confinement times with experimental data reveals a challenge: while experimental particle and energy fluxes naturally increase towards the edge, neoclassical fluxes exhibit a pronounced decrease due to the increased collisionality, see Fig. 6, left. Thus, confinement times diverge towards the plasma edge. This issue is not severe because neoclassical theory is not applicable to TJ-II plasma edge parameters. To partially address this concern, the smallest neoclassical particle and energy confinement times, typically observed in the gradient region around r/a=2/3, are compared with the experimental and the ISS04 scaling law values, as shown in Table I. Due to the transient values of the diamagnetic energy W=W(t) for the reference discharge without pellets #55298 and the one with two pellets #55313, see Fig. 1, bottom, the experimental energy confinement times are calculated with $\tau_E=W/(P-dW/dt)$, resulting in an approximate 20% increase in the results for these discharges.

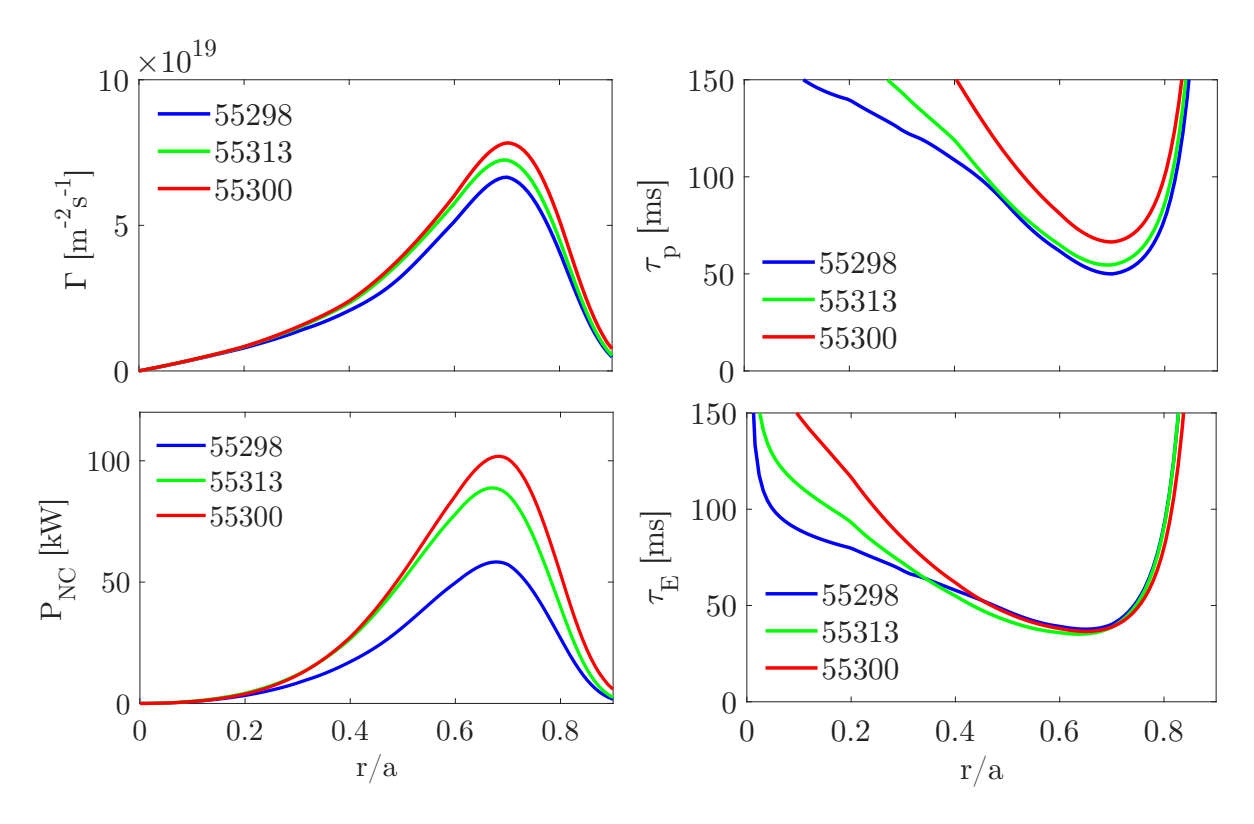


FIG. 6. Profiles of the neoclassical particle flux Γ (top left), particle confinement time τ_p (top right), neoclassical heat flux Q (bottom left) and energy confinement time τ_e , (bottom right for the reference discharge without pellets, #55298 (blue) and with one #55313 (green) and two #55300 (red) pellets.

With a total NBI input power of $P_{NBI}=320~{\rm kW}$, the neoclassical energy flux accounts for only 50 kW of power loss in the reference discharge #55298, increasing to 100 kW in the two-pellets case #55300, see Fig. 6, bottom left. Other mechanisms must be responsible of the particle and energy transport, particularly for a stellarator with a substantial plasma wall interaction and a complex magnetic structure like TJ-II. Nevertheless, it is noteworthy that in both experimental and neoclassical results the energy confinement time does not vary significantly between discharges, despite the plasma energy nearly doubling and the ion temperature increasing by 50%. The explanation in the neoclassical simulations is straightforward. The energy content W doubles, the neoclassical power loss P_{NC} doubles, and consequently, the energy confinement time τ_E^{NC} must be roughly the same, Fig. 6, bottom right. The transition between the onset of the Pfirsch-Schlüter regime and the plateau regime and their different temperature scalings is the responsible for the mild dependence, see Fig. 5.

TABLE 1. COMPARISON BETWEEN EXPERIMENTAL RESULTS AND NEOCLASSICAL SIMULATIONS FOR THE REFERENCE DISCHARGE WITHOUT PELLETS, #55298 AND WITH ONE #55313 AND TWO #55300 PELLETS.

Shot	$W_{\rm diag}[kJ]$	$ au_{ m E}^{ m exp}[{ m ms}]$	$ au_{ m E}^{ m ISS04}[{ m ms}]$	$ au_{ m E}^{ m NC}[{ m ms}]$	$ au_{ m p}^{ m NC}[m ms]$	$I_b[kA]$	$I_p[kA]$	$I_{NBI} + I_b[kA]$
#55298	2.4	10.2	7.5	38	50	0.6	-1.5	-1.5
#55313	3.6	13.3	11.3	35	54	1.0	-1.2	-1.1
#55300	4.4	13.8	12.6	36	66	1.2	-0.8	-0.9

For these series of discharges, plasmas are heated with the counter NBI system of TJ-II. Consequently, the measured total plasma current I_p includes both bootstrap and NBI-driven components. By subtracting the neoclassical bootstrap current estimate I_b from the measured I_p of the reference discharge #55298, an NBI current $I_{NBI} = I_p - I_b = -2.1$ kA was estimated. Assuming I_{NBI} remains constant across all discharges -a significant assumption- this calculation yields results consistent with the experimentally measured current, exhibiting a discrepancy of only 0.1 kA ($\approx 10\%$), Table I, last two columns.

3. SUMMARY

An enhanced confinement regime is induced by multi-pellet injection in NBI-heated plasmas at TJ-II. This is clearly observed in the series of discharges analyzed here, heated with $P_{NBI}=320~{\rm kW}$, and where the diamagnetic energy content increases from 2.4 kJ in gas puffing only operation, #55298, to 3.6 kJ with one pellet, #55313, and 4.4 kJ with two pellets, #55300. The substantial increase in ion temperature resulting from multi-pellet injection effectively mitigates neoclassical diffusion by transitioning the ion collisionality from the Pfirsch-Schlüter towards the plateau regime. This, in conjunction with the measured reduction in density and electrostatic potential fluctuations, suggesting reduced turbulent transport [13,14], partially explains the observed enhanced plasma performance in NBI-heated TJ-II conditions. A systematic comparison between experimental measurements and simulations, including turbulent, neoclassical and ASTRA [15] models, is currently underway to quantify the contribution of these transport channels.

ACKNOWLEDGEMENTS

This research was partially financed by grants PID2022-137869OB-I00, PID2020-116599RB-I00 and PID2023-148697OB-I00 funded by MICIN/AEI/10.13039/501100011033, by "ERDF A way of Making Europe", and by the European Union through the Euratom Research and Training Programme (Grant Agreement No 101052200 - EUROfusion). The views and opinions expressed herein are solely those of the author(s) and do not necessarily reflect those of the European Union or the European Commission, which can hold no responsibility for them. Furthermore, computational resources were provided by Uranus supercomputer cluster located at UC3M, which was jointly financed by EU FEDER funds and by the Spanish National Research Project No. UNC313-4E-23612, ENE2009-12213-C03-03, ENE2012-33219, and ENE2012- 31753.

REFERENCES

- [1] GARCÍA-CORTÉS, I., *et al*, Enhanced confinement induced by pellet injection in the stellarator TJ-II, Phys. Plasmas **30** (2023) 072506.
- [2] McCARTHY, K.J., *et al*, Multi-pellet injection into the NBI-heated phase of TJ-II plasmas, Nucl. Fusion **64** (2024) 066019.
- [3] McCARTHY, K.J., *et al*, Comparison of cryogenic (hydrogen) and TESPEL (polystyrene) pellet particle deposition in a magnetically confined plasma, Europhys. Lett. **120** (2017) 25001.
- [4] PANADERO, N., *et al*, Experimental studies and simulations of hydrogen pellet ablation in the stellarator TJ-II, Nucl. Fusion **58** (2018) 026025.
- [5] McCARTHY, K.J., *et al*, Plasma fueling with cryogenic pellets in the stellarator TJ-II, Nucl. Fusion **57** (2017) 056039.

- [6] YAMADA, H., *et al*, Characterization of energy confinement in net-current free plasmas using the extended International Stellarator Database, Nucl. Fusion **45** (2005) 1684.
- [7] THIENPONDT, H., *et al*, Influence of the density gradient on turbulent heat transport at ion-scales: an inter-machine study with the gyrokinetic code stella, Nucl. Fusion **65** (2025) 016062.
- [8] BEIDLER, C.D., *et al*, Benchmarking of the mono-energetic transport coefficients results from the International Collaboration on Neoclassical Transport in Stellarators (ICNTS), Nucl. Fusion **51** (2011) 076001.
- [9] TURKIN, Y., et al, Neoclassical transport simulations for stellarators, Phys. Plasmas 18 (2011) 022505.
- [10] TRIBALDOS, V., *et al*, Extended estimations of neoclassical transport for the TJ-II stellarator: The bootstrap current, Phys. Plasmas **18** (2011) 102507.
- [11] HIRSHMAN, S.P., *et al*, Plasma transport coefficients for nonsymmetric toroidal confinement systems, Phys. Fluids **29** (1986) 2951. RIJ, W.I., van and HIRSHMAN, S.P., Variational bounds for transport coefficients in three-dimensional toroidal plasmas, Phys. Fluids B **1** (1989) 563.
- [12] MAASSBERG, H., BEIDLER, C.D., TURKIN, Y., Momentum correction techniques for neoclassical transport in stellarators, Phys. Plasmas **16** (2009) 072504.
- [13] GARCÍA-CORTÉS, I. *et al*, Exploring enhanced plasma performance after pellet injections via rotational transform modulation in the TJ-II Stellarator, at this conference, IAEA-CN-316-2803.
- [14] GARCÍA-REGAÑA, J.M., *et al*, Transport in high-performance plasmas of the TJ-II Stellarator: From first-principles simulation to experimental validation, at this conference, IAEA-CN-316-2902.
- [15] PEREVERZEV, G.V., and YUSHMANOV, P.N., Internal report, ASTRA Automated System for TRansport Analysis IPP-Report, IPP 5/98 2002.